NUMERICAL SOLUTION OF THE MAGNETIC RELIEF PROBLEM–A PRELIMINARY REPORT

Katarzyna Jonca and Curtis R. Vogel[1]

1 INTRODUCTION

In this paper we discuss the numerical solution of an inverse problem arising in geophysics. The physical problem is to determine the location of buried magnetized rock from measurements of the magnetic field taken at the surface. Koch and Tarlowski [3] have derived a mathematical model which leads to a system of nonlinear first kind integral equations. This system can be formulated as an operator equation

$$K(f) = g \tag{1.1}$$

where the operator K is nonlinear and maps a Hilbert space X into a Hilbert space Y. The solution f to (1.1) represents the location of the buried magnetized rock, while g represents magnetic field measurements. A discussion of the physical problem and the mathematical model appears in section 2.

This problem is ill-posed. To approximately solve it, Tikhonov Regularization is used, i.e., one solves

$$\min_{f \in X} \{ \|K(f) - g\|^2 + \alpha \|f\|^2 \} \tag{1.2}$$

for a sequence of values of the regularization parameter α. Ill-posedness, regularization, and the practical choice of the spaces X and Y and the choice of the regularization parameter α using Generalized Cross Validation (GCV) are considered in section 3.

Section 4 contains a detailed description of a robust iterative algorithm to solve problem (1.2). To obtain numerical stability, we apply the Singular Value Decomposition of the derivative operator. This also allows easy computation of the GCV functional. A trust region approach is used to guarantee convergence of the iteration. Numerical results are presented in section 5.

2 THE MATHEMATICAL MODEL

Experimental evidence suggests that in certain situations the variations in magnetic field of the earth depend primarily on the shape of the boundary between magnetized igneous rock and unmagnetized sediments, which cover this rock. One wishes to determine this shape from airborne magnetic data. The mathematical formulation of the relationship between the variations in the magnetic field and the shape and location of

[1]This research was partially supported by the NSF under Grant DMS-8602000. Initial work was done during the second author's visit to the Centre for Mathematical Analysis at the Australian National University, Canberra, Australia, with support through the Centre. Work was completed at Montana State University.

the boundary leads to a system of nonlinear first kind integral equations. A derivation of this system appears in [3].

Let the z-axis be chosen so that the positive z direction is downward, and the measurements of the magnetic field $\mathbf{H}$ take place in the plane $z = 0$. Let the boundary surface σ have the parameterization

$$\sigma = \{(x, y, z) : z = h + f(x, y), -\infty < x < \infty, -\infty < y < \infty\}, \tag{2.1}$$

where h is the average depth of the surface (see Figure 1 below) and Ω is the (horizontal) x-y plane. We refer to f as the relief function. Assuming constant magnetization $\mathbf{M} = [M_x, M_y, M_z]^T$ of the igneous rock and outward unit normal $\mathbf{n}$ to the surface σ, the intensity of the measured magnetic field is given by

$$\mathbf{H}(s,t,0) = -\int_\sigma \mathbf{M}\cdot\mathbf{n}\,\nabla\frac{1}{\|(s,t,0)-(x,y,z)\|}\,dS \tag{2.2}$$

$$= -\int \frac{(M_x\frac{df}{dx} + M_y\frac{df}{dy} - M_z)[s-x, t-y, -h-f(x,y)]}{\{(s-x)^2+(t-y)^2+(h+f(x,y))^2\}^{3/2}}\,dx\,dy.$$

Subscripts "x" and "y" indicate horizontal components, while "z" indicates the vertical component. Integration is performed over the x-y plane.

Figure 1

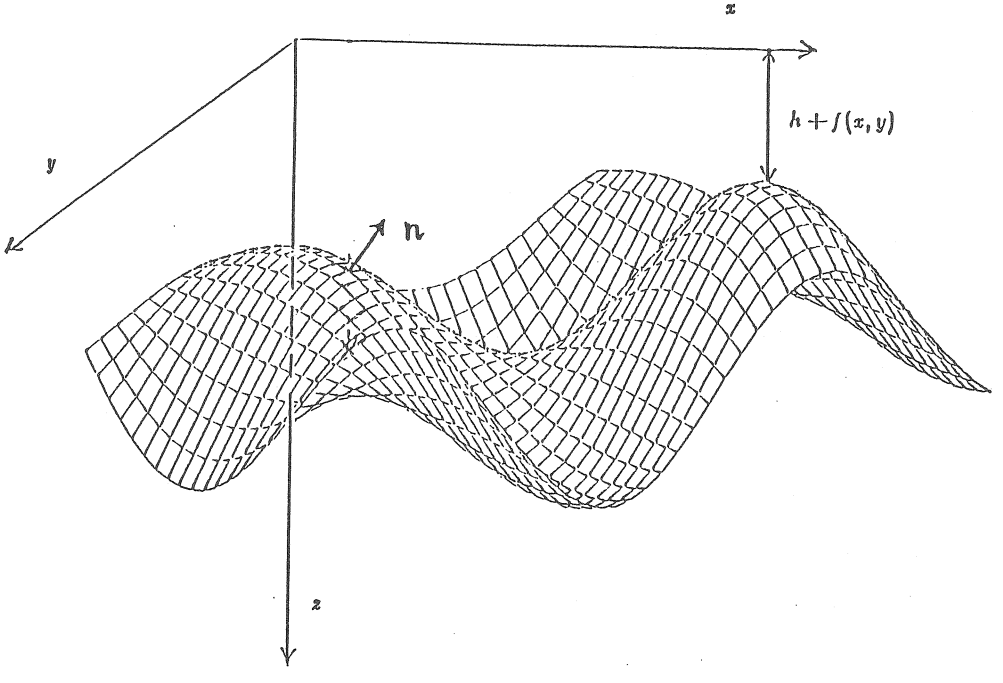

Letting g_x, g_y, g_z denote the components of $\mathbf{H}$, the following system of nonlinear first kind integral equations must be solved to obtain f:

$$g_x(s,t) = \int \frac{(M_x \frac{df}{dx} + M_y \frac{df}{dy} - M_z)(s-x)}{\{(s-x)^2 + (t-y)^2 + (h+f(x,y))^2\}^{3/2}} dxdy \tag{2.3}$$

$$g_y(s,t) = \int \frac{(M_x \frac{df}{dx} + M_y \frac{df}{dy} - M_z)(t-y)}{\{(s-x)^2 + (t-y)^2 + (h+f(x,y))^2\}^{3/2}} dxdy \tag{2.4}$$

$$g_z(s,t) = \int \frac{(M_x \frac{df}{dx} + M_y \frac{df}{dy} - M_z)(-h-f(x,y))}{\{(s-x)^2 + (t-y)^2 + (h+f(x,y))^2\}^{3/2}} dxdy \tag{2.5}$$

Since the relief function f depends on 2 variables, we refer to this case as the 2-D magnetic relief problem.

A less realistic but computationally much simpler problem arises when the relief function f is assumed to be independent of the y coordinate, and only measurements of the vertical component g_z of the magnetic field are taken. One then obtains a single integral equation with an unknown relief function $f(x)$, dependent on one variable only, which we refer to as the 1-D magnetic relief problem. The scalar analogue of the system (2.3)-(2.5) is then

$$g_z(s) = 2 \int \frac{(M_x f'(x) - M_z)(-h-f(x))}{(s-x)^2 + (h+f(x))^2} dx \tag{2.6}$$

where the integration is now over the x-axis.

We will assume that f is identically zero outside a smooth bounded domain Ω, and that measurements $g(s,t)$ are taken only at points $(s,t) \in \Omega$. The components of g can be suitably modified so that the integration above takes place over this restricted domain Ω rather than over the entire x-y plane (or x-axis, in the 1-D case). Thus, the problem can be formulated as a nonlinear operator equation (1.1), with

$$K(f) := \int_\Omega k(\cdot, x, f(x)) dx. \tag{2.7}$$

The components of the kernel k are given in the 2-D case by the right hand sides in (2.3)-(2.5) and in the 1-D case by the right hand side in (2.6). g is a function whose components represent measurements of the magnetic field $\mathbf{H}$.

3 ILL-POSEDNESS AND REGULARIZATION

Given an arbitrary $g \in Y$, the problem of finding an $f \in X$ such that $K(f) = g$ is *well-posed* provided: (i) for any $g \in Y$, there exists a solution $f \in X$ such that $K(f) = g$; (ii) the solution f is unique; (iii) the solution f depends continuously on the data g.

The well-posedness of this particular inverse problem depends on the choice of the spaces X and Y. From the physical point of view it seems appropriate to assume that the solution f is "smooth" in the sense that f is differentiable and

$$\|f\|^2 := \int_\Omega \nabla f(x) \cdot \nabla f(x) dx \tag{3.1}$$

is bounded. Since we have also assumed that f vanishes outside Ω, we choose the Hilbert space $X = H_0^1(\Omega)$ consisting of functions f in the Sobolev space $H^1(\Omega)$ satisfying the boundary condition $f(x) = 0$, $x \in \partial\Omega$, with inner product

$$< f, h >= \int_\Omega \nabla f(x) \cdot \nabla h(x) dx, \qquad f, h \in X. \tag{3.2}$$

Thus (3.1) gives the induced norm on X.

On the other hand the components of g come from measurements at discrete points in Ω. One cannot assume that the derivatives of these components are available. Thus an appropriate choice for Y in the 1-D case is $L^2(\Omega)$. In the 2-D case, since measurements have 3 components, we will consider $Y = [L^2(\Omega)]^3 := L^2(\Omega) \times L^2(\Omega) \times L^2(\Omega)$.

With this physically reasonable choice of spaces X and Y problem (1.1) is ill-posed. Clearly the components of the kernel k are smooth in s, and hence, for any $f \in X$, the components of $K(f)$ are smooth. Therefore there exist elements $g \in Y$ for which (1.1) has no solution. Perhaps a more serious difficulty is that small perturbations in the data $g \in Y$ may give rise to arbitrarily large perturbations in solutions $f \in X$.

Obtaining approximate solutions to an ill-posed problem requires regularization. Using the method of Tikhonov Regularization [6], we replace the ill-posed problem (1.1) by a sequence of regularized (i.e., stabilized) problems

$$\min_{f \in X} \{\|K(f) - g\|^2 + \alpha \|f\|^2\} \tag{3.3}$$

For a discussion of existence and stability of solutions f_α to (3.3) and convergence of these solutions as the regularization parameter $\alpha \to 0$ and as the perturbations in the data tend to zero, see [5].

A very important practical point consideration is choice of the regularization parameter α for a given (error contaminated) data set. One would like to be able to choose α so that $\|f_\alpha - f\|$ is minimized, where f is the (unknown) true solution. If the error in the data is random, under certain conditions (e.g., see [7]) the method of Generalized Cross Validation (GCV) yields a probabilistic indicator of the size of $\|K(f_\alpha) - K(f)\|^2$, which is related to $\|f_\alpha - f\|$. For Tikhonov Regularization, this indicator is given by the GCV function

$$V(\alpha) = \frac{\|K(f_\alpha) - g\|^2}{Trace[I - A(A^T A + \alpha I)^{-1} A]}, \tag{3.4}$$

where $A = K'(f_\alpha)$ is the derivative operator defined in the following remark. For an application of GCV to a nonlinear integral equation arising in the remote sensing of the atmosphere, see [4].

Remark. $K : X \to Y$ in (2.7) is Frechet differentiable. In the 1-D case, the derivative operator $K'(f) : X \to Y$ is defined by

$$K'(f)u(s) = 2 \int_\Omega \frac{-h - f(x)}{(s-x)^2 + (h + f(x))^2} M_z u'(x) dx \tag{3.5}$$

$$+2 \int_\Omega (M_z f'(x) - M_z) \frac{-(s-x)^2 + (h + f(x))^2}{[(s-x)^2 + (h + f(x))^2]^2} u(x)\, dx$$

In the 2-D case the components of the derivative have a similar form. For example, the x-component of $K'(f)u$ is given by

$$(3.6)\qquad \int_\Omega \frac{(s-x)\times(M_x\frac{du}{dx}+M_y\frac{du}{dy})}{[(s-x)^2+(t-y)^2+(h+f(x,y))^2]^{3/2}}dxdy$$
$$+\int_\Omega \frac{(M_x\frac{du}{dx}+M_y\frac{du}{dy}-M_z)\times -3(s-x)(h+f(x,y))}{[(s-x)^2+(t-y)^2+(h+f(x,y))^2]^3}dxdy$$

4 NUMERICAL IMPLEMENTATION

In our numerical implementation we took approximate solutions $f_n(x)$ from the n-dimensional subspace of $X = H_0^1(\Omega)$ spanned by basis functions $\{\phi_j(x)\}_{j=1}^n$. In the 1-D case, simulated measurements g_i were taken at m points $s_i \in \Omega$. We assume $m \geq n$. The square of the L^2 norm, $\|K(f_n)-g\|^2$, was approximated by the weighted discrete sum

$$(4.1)\qquad \frac{1}{m}\sum_{i=1}^{m}[K(f_n)(s_i)-g_i]^2$$

The operators K and K' were replaced by discrete operators K_{mn}, K'_{mn}, which we now introduce.

Given the coefficient vector $c=[c_j]\in R^n$, define

$$(4.2)\qquad f_n(x)=\sum_{j=1}^{n}c_j\phi_j(x)\in X.$$

Then from (2.6), $K_{mn}: R^n \to R^m$ is given by

$$(4.3)\qquad [K_{mn}(c)]_i = K(f_n)(s_i), \qquad 1\leq i\leq m, c\in R^n.$$

From (3.5) the derivative $K'_{mn}(c)$ has the $m\times n$ matrix representation

$$(4.4)\qquad [K'_{mn}(c)]_{ij} = K'(f_n)\phi_j(s_i), \qquad 1\leq i\leq m, 1\leq j\leq n.$$

The integrals in (4.3) and (4.4) were evaluated using panel Gaussian quadrature. The operators in the 2-D case are analogous, but somewhat more complicated. For example, (2.3)-(2.5) defines an operator K with three components, and hence, the discretized operator maps coefficients in R^n to a data vector of size $m=3p$, where p is the number of points $(s,t)\in\Omega$ at which measurements are taken.

From (3.1), the penalty term $\|f\|^2$ in (3.3) yields the quadratic form

$$\|f_n\|^2 = c^T B_n c,$$

where B_n is the symmetric positive definite $n\times n$ matrix with components

$$(4.5)\qquad [B_n]_{ij}=\int_\Omega \nabla\phi_i(x)\cdot\nabla\phi_j(x)dx, \qquad 1\leq i,j\leq n.$$

The finite dimensional analogue of the problem (3.3) is

$$\min_{c\in R^n}\{\frac{1}{m}\sum_{i=1}^{n}([K_{mn}(c)]_i - g_i)^2 + \alpha c^T B_n c\}. \tag{4.6}$$

To solve this minimization problem, a quasi-Newton/trust region method is used. For notational convenience, we drop the subscripts and multiply the objective function in by $\frac{m}{2}$. "$\|\cdot\|$" indicates the usual Euclidean norm in R^m or R^n. Since B is symmetric positive definite, we can take its Choleski factorization $B = R^T R$, where R is upper triangular. The objective function for problem (4.6) becomes

$$T_\alpha(c) := \frac{1}{2}\{\|K(c) - g\|^2 + m\alpha\|Rc\|^2\} \tag{4.7}$$

A necessary condition for a minimum, the gradient (first derivative) equals zero, gives

$$G(c) := K'(c)^T[K(c) - g] + m\alpha Bc = 0 \tag{4.8}$$

The Hessian (second derivative) of the objective function is

$$H(c) := K''(c)^T[K(c) - g] + K'(c)^T K'(c) + m\alpha B \tag{4.9}$$

Due to the expense in computing $K''(c)$, we approximate the Hessian by the positive definite matrix

$$\hat{H}(c) := K'(c)^T K'(c) + m\alpha B \tag{4.10}$$

The quasi-Newton iteration

$$c_{k+1} = c_k - \hat{H}(c_k)^{-1}G(c_k), \qquad k = 0, 1, \ldots, \tag{4.11}$$

will converge to a (local) minimizer c_* of (4.7) provided $H(c_*)$ is positive definite and the initial guess c_0 is sufficiently close to c_*. Otherwise, the iteration may not converge or it may converge to a solution to $G(c) = 0$ which is not a local minimizer.

To obtain convergence to a minimizer under much weaker conditions, a trust region approach [1] is used. Iteration (4.11) is replaced by

$$c_{k+1} = c_k + s_k, \tag{4.12}$$

where s_k solves the constrained minimization problem

$$\min_{s\in R^n}\{\|K(c_k) + K'(c_k)s - g\|^2 + m\alpha\|c_k + s\|^2\} \tag{4.13}$$

$$\text{subject to } \|s\| \le \delta_k,$$

and the trust region radius δ_k is chosen to obtain sufficient decrease in $T_\alpha(c)$ at each iteration to guarantee convergence.

To solve (4.13), we use an approach similar to that of Elden [2]. The problem is first diagonalized using the Singular Value Decomposition (SVD). Then a standard dual space technique is used to solve the diagonalized problem. This approach is numerically

stable, quite efficient, and it allows easy computation of the GCV function in (3.4). We assume $m \geq n$.

Let

$$b := g - K(c_k),$$
$$A := K'(c_k)R^{-1},$$

and let A have the SVD

$$A = UDV^T, \quad U_{m\times m}, V_{n\times n} \text{ orthogonal}, D_{m\times n} = diag\{d_i\}.$$

Consider the change of variables

$$\hat{s} = V^T R s, \quad \hat{c} = V^T R c_k, \quad \hat{b} = U^T b. \tag{4.14}$$

Then (4.13) is equivalent to the diagonalized problem

$$\min_{\hat{s}\in R^n}\{\|D\hat{s} - \hat{b}\|^2 + \alpha\|\hat{c} + \hat{s}\|^2\} \quad \text{subject to } \|\hat{s}\|^2 \leq \delta_k^2. \tag{4.15}$$

The unique solution to problem (4.15) has the form

$$\hat{s} = \hat{s}(\mu) = \{D^T D + (\alpha + \mu)I\}^{-1}(D\hat{b} - \alpha\hat{c}), \tag{4.16}$$

where $\mu \geq 0$ is a Lagrange multiplier. If $\|\hat{s}(0)\| \leq \delta_k$, then $s = R_{-1}V\hat{s}(0)$ solves (4.13). Otherwise the constraint is active, and $s = R^{-1}V\hat{s}(\mu)$ solves (4.13), where $\mu \geq 0$ is the unique solution to

$$g(\mu) := \|\hat{s}(\mu)\|^2 - \delta_k^2 = 0. \tag{4.17}$$

We solve (4.17) using the algorithm given in [1], which requires $g(\mu)$ and its derivative $g'(\mu)$. In terms of the singular values d_i and the components of $\hat{b}$ and $\hat{c}$,

$$g(\mu) = \sum_{i=1}^{n} \frac{(d_i\hat{b}_i - \alpha\hat{c}_i)}{(d_i^2 + \alpha + \mu)}^2 - \delta_k^2, \tag{4.18}$$

so both g and g' can be obtained easily. The GCV function is computed using

$$V(\alpha) = \frac{\frac{1}{m}\|K(c_\alpha) - g\|^2}{[\frac{m-n}{m} + \sum_{i=1}^{n} \frac{\alpha}{(d_i^2+m\alpha)}]^2}, \tag{4.19}$$

where c_α solves (4.6).

To determine the trust region radius δ_k, we used the algorithm in [1], p. 143. The basic idea is to pick δ_k such that the objective function $T_\alpha(c)$ decreases sufficiently, i.e.,

$$T_\alpha(c_k + s) \leq T_\alpha(c_k) + \epsilon G(c_k)^T s, \tag{4.20}$$

where ϵ is a small positive parameter. Note that

$$\|s\|^2 \to 0 \text{ as } \delta_k \to 0,$$
$$T_\alpha(c_k + s) = T_\alpha(c_k) + G(c_k)^T s + O(\|s\|^2),$$

and

$$\begin{aligned} G(c_k)^T s &= -G(c_k)^T [K'(c_k)^T K'(c_k) + (m\alpha + \mu)B]^{-1} G(c_k) \\ &\leq -\frac{\|R^{-T} G(c_k)\|^2}{(d_{max}^2 + m\alpha + \mu)}, \end{aligned}$$

where d_{max} is the maximum singular value of $A = F'(c_k)R^{-1}$. Thus requirement (4.20) can be fulfilled provided the gradient $G(c_k)$ is nonzero and δ_k is sufficiently small.

In addition, δ_k is chosen so that we "trust" the quadratic approximation to $T_\alpha(f)$ within the trust region, i.e.,

$$T_\alpha(c_k + s) \approx T_\alpha(c_k) + G(c_k)^T s + \frac{1}{2} s^T \hat{H} s \quad \text{whenever } \|s\| \leq \delta_k. \tag{4.21}$$

This requirement allows us to increase the size of the step s under certain conditions, thereby increasing the rate of convergence for iteration (4.12)-(4.13).

5 NUMERICAL RESULTS

We first present results for the 1-D magnetic relief problem with computational domain $\Omega = (0, 1)$ and magnetization vector $\mathbf{M} = [M_x, M_y, M_z]^T = [1, 1, 1]^T$. We conducted a linearized stability analysis about $f_0 = 0$ to determine how the resolution (i.e., the accuracy of approximation to the solution) varies as the depth h increases. From physical arguments, one might expect good resolution for small h, with decreasing resolution as the depth h increases. Since

$$K(f_0 + \Delta f) - g \approx K(f_0) + K'(f_0)\Delta f - g, \tag{5.1}$$

this can be analyzed by examining the derivative operator $K'(f_0)$. Recall that from (2.6), the nonlinear integral operator K has as its kernel

$$k(s, x, f, f') = \frac{2(M_x f'(x) - M_z)(-h - f(x))}{(s - x)^2 + (h + f(x))^2}.$$

In (3.5), the derivative operator $K'(f)$ is expressed as the sum of two linear integral operators. Given $u \in H^1(\Omega)$, the first is applied to $u'(x)$ and has as its kernel

$$\frac{\partial k}{\partial f'} = \frac{-2M_x(h + f(x))}{(s - x)^2 + (h + f(x))^2}. \tag{5.2}$$

The second integral operator is applied to $u(x)$ and has as its kernel

$$\frac{\partial k}{\partial f} = \frac{2(M_x f'(x) - M_z)(-(s-x)^2 + (h+f(x))^2)}{[(s-x)^2 + (h+f(x))^2]^2}. \tag{5.3}$$

Figure 2 below shows plots of minus one half the first kernel (5.2) evaluated at $f = f_0 = 0$, $M_x = M_z = 1$, and fixed $s = \frac{1}{2}$. The solid line was obtained for depth $h = 0.1$, while the dotted line represents $h = 0.2$. Similar graphs for the second kernel (5.3) appear in Figure 3. One sees from these two plots that the kernels become more "flat" and less "delta-like" as the depth h increases.

Figure 2

$-\frac{1}{2} \times \frac{\partial k}{\partial f'}$ at $f = 0, M_x = M_z = 1, s = \frac{1}{2}$ for $h = 0.1$ and $h = 0.2$

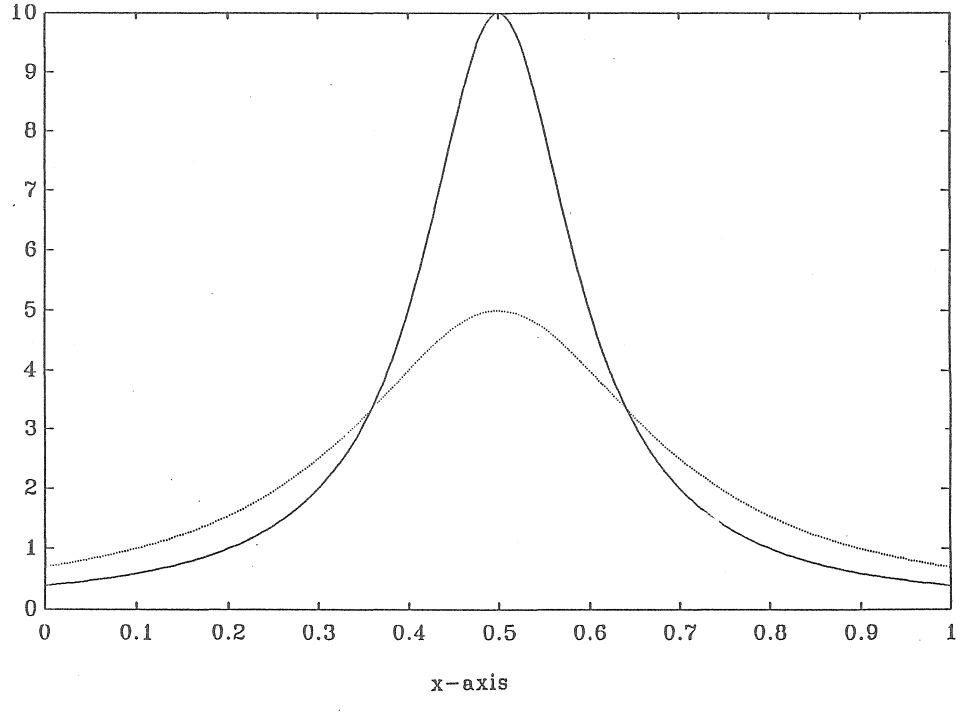

Figure 3

$-\frac{1}{2} \times \frac{\partial k}{\partial f}$ at $f = 0, M_x = M_z = 1, s = \frac{1}{2}$ for $h = 0.1$ and $h = 0.2$

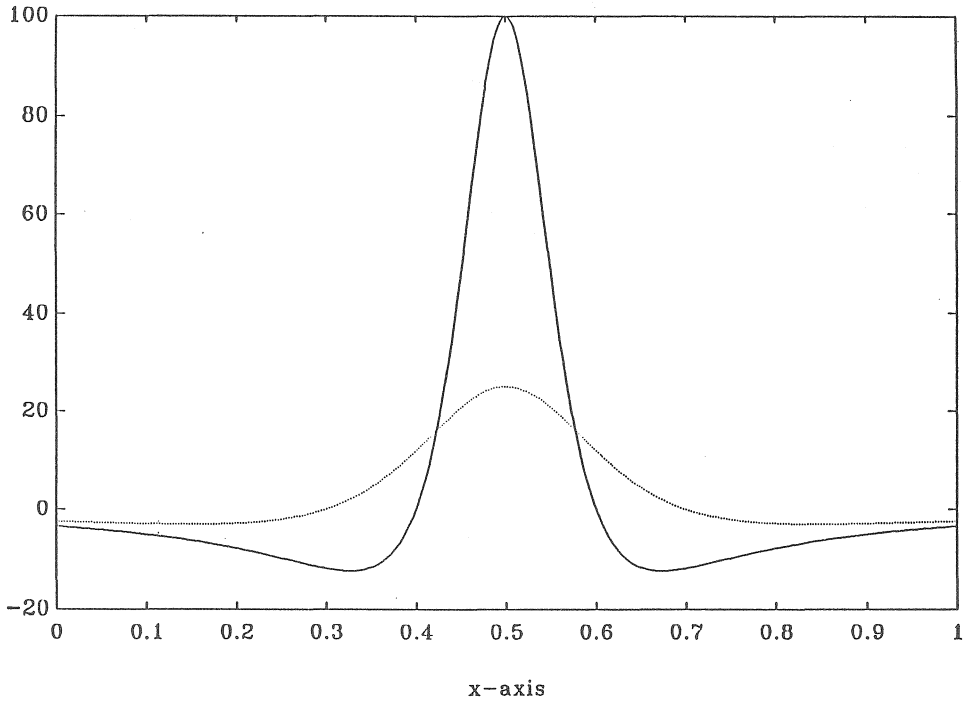

A quantitative description of how increasing depth decreases the resolution is given in Figure 4. Here we plot the singular values in order of decreasing magnitude for the derivative operator $K'(c)$ defined in (4.4) for both $h = 0.1$ (stars) and $h = 0.2$ (circles). We took the functions $\{\phi_j\}_{j=1}^n$, $n = 15$, to be cubic spline basis functions (B-splines) with equally spaced nodes in the interval $(0, 1)$.

Figure 4

Singular Values of the Derivative

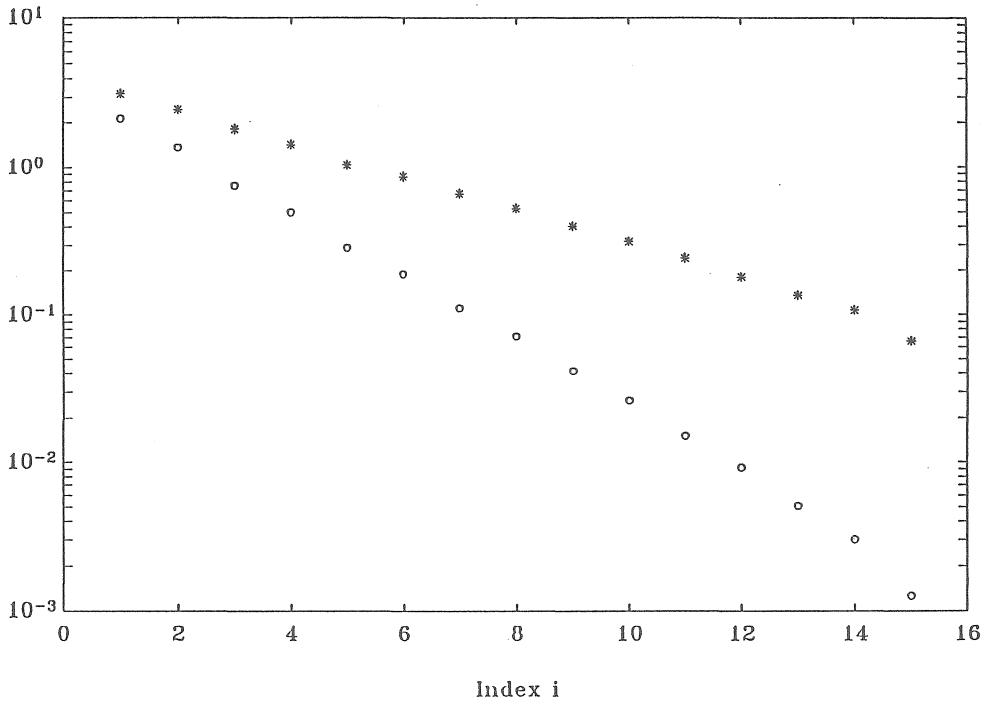

In the above graph, both sets of singular values appear to decay exponentially (note logarithmic scale), i.e., the i^{th} singular value appears to have the behavior

$$\sigma_i \approx c\exp(-\beta i), \quad i = 1, 2, \ldots, \; c > 0, \beta > 0. \tag{5.4}$$

As the depth h increases, the constant β increases. Thus the singular values decay more rapidly with increasing depth. Since Tikhonov Regularization has the effect of filtering out components associated with small singular values, it should come as no surprise that the amount of resolution for the (regularized) solutions should decrease with increased depth.

We next generated synthetic data $g_i = K(f)(s_i)$ and obtained approximate solutions using the implementation of Tikhonov Regularization described in section 4. The true magnetic relief function was taken to be a linear combination of Gaussians:

$$-f(x) = a_1\exp(-d_1(x - x_1)^2) + a_2\exp(-d_2(x - x_2)^2) \tag{5.5}$$

The parameters $a_1 = .1, a_2 = .05$ control the magnitude of the solution. $d_1 = 60, d_2 = 40$ determine the rate of decay of the Gaussians, and $x_1 = .33, x_2 = .66$ specify the locations of the peaks. We generated $m = 50$ data points $g_i = g(s_i), s_i = \frac{i}{m-1}, i =$

$0, 1, \ldots, m-1$. To the data g_i we added pseudo-random error ϵ_i with a $N(0, \sigma^2 I)$ distribution. The standard deviation σ was picked so that

$$\frac{\sqrt{E\|\epsilon\|^2}}{\|g\|} = .01.$$

We used $n = 15$ B-spline basis functions, each of which satisfied the boundary conditions $\phi_j(0) = \phi_j(1) = 0$, to approximate the true solution. We solved the resulting finite dimensional minimization problem (4.6) for a decreasing sequence of regularization parameters $\alpha = 10^{-p}, p = 0, 1, \ldots, 5$. The resulting approximations are shown in Figure 5. The +'s represent the true solution, the o's represent the regularized solution for $\alpha = 10^0 = 1$, the solid curve represents the regularized solution for $\alpha = 10^{-2}$, and the dotted curve represents the regularized solution for $\alpha = 10^{-5}$.

Figure 5

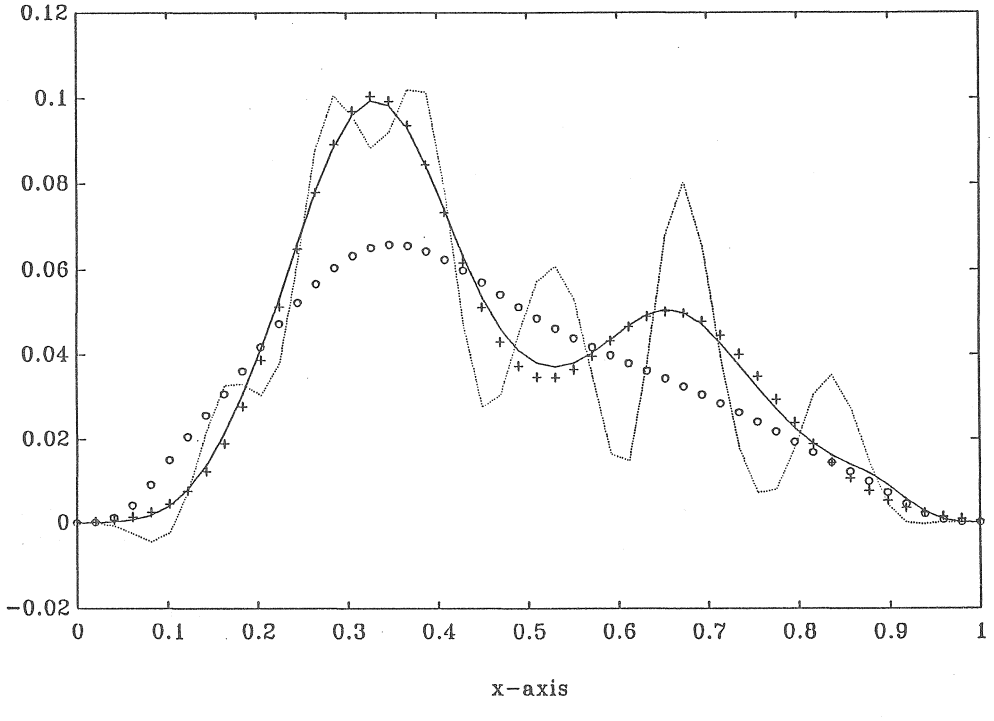

Figure 6 shows the norm of the true error $\|e_\alpha\| = \|f_\alpha - f\|$ (indicated by stars) and the GCV functional (indicated by o's) as functions of α. Note that the true error increases sharply as α becomes very small. On the other hand, the GCV stays very flat.

Figure 6
$\|e(\alpha)\|$ and $V(\alpha)$ vs α

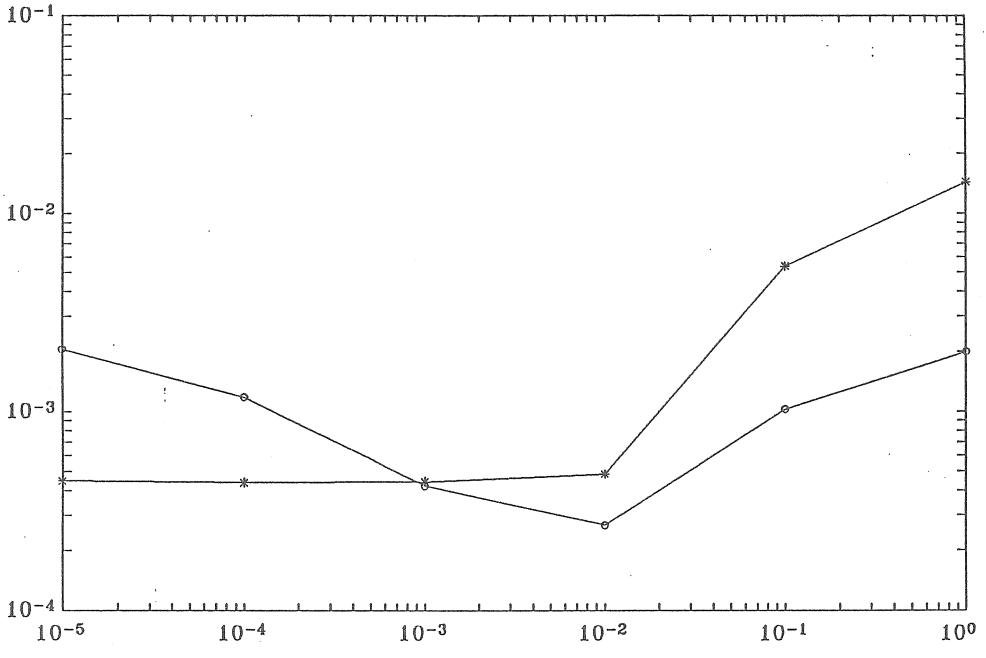

We also have some preliminary results for the 2-D magnetic relief problem. Although this problem is conceptually quite similar to the 1-D problem, it is computationally much more difficult due to the greater number of basis functions required to represent 2-D solutions and the integration required over 2 space dimensions. The computations for the 1-D problem were performed on a Zenith (IBM-compatible) PC. The 2-D computations required a CRAY X-MP supercomputer. Figure 7 shows a regularized approximation to

$$-f(x,y) = a_1 \exp(-d_1(x-x_1)^2 - e_1(y-y_1)^2) + a_2 \exp(-d_2(x-x_2)^2 - e_2(y-y_2)^2), \tag{5.6}$$

with parameters $a_1 = .05, a_2 = .03, d_1 = d_2 = e_1 = e_2 = 60, x_1 = y_1 = .4, x_2 = y_2 = .6$. As in the 1-D example, the depth h was taken to be 0.2. The error was also chosen as in the 1-D case, and we took the same sequence of regularization parameters α. We took basis functions to be tensor products of cubic splines. A total of $64 = 8^2$ B-spline tensor product basis functions and $225 = 15^2$ data points were used on the unit square $\Omega = (0,1) \times (0,1)$. The approximation in Figure 7 is for $\alpha = 10^{-3}$.